Applied Clay Science 281 (2026) 108067

Contents lists available at ScienceDirect

Applied Clay Science

journal homepage: www.elsevier.com/locate/clay

Research paper

Swelling behaviour of compacted Ca/Mg bentonite during hydration on different scales☆

Antonia Nitsch [a,*], Ali Asaad [b], Torsten Wichtmann [a], Katja Emmerich [b], Wiebke Baille [a]

[a] Chair of Soil Mechanics, Foundation Engineering and Environmental Geotechnics, Department of Civil and Environmental Engineering, Ruhr-Universität Bochum, Bochum, Germany

[b] Institute of Concrete Structures and Building Materials (IMB/MPA/CMM), Karlsruhe Institute of Technology (KIT), Karlsruhe, Germany

ARTICLE INFO

Keywords:
Laboratory scale mock-up test
Swelling pressure
Bentonite
Engineered barrier systems

ABSTRACT

A mock-up test on decimetric scale in an innovative column test device and small-scale element tests were carried out on a German Ca/Mg bentonite, which is investigated as a suitable material for engineered barrier systems in nuclear waste disposal. Key hydro-mechanical parameters such as relative humidity, water content and swelling pressure were monitored and spatially resolved over the 30 cm height of the column in the mock-up test. The test was hydrated from the bottom and ran for 370 days. To compare the material behaviour at different scales, swelling pressure tests and water retention measurements were performed at the element-test scale. The results of the column test showed a heterogeneous evolution of swelling pressure and hydration state variables along the column height. Simultaneous measurement of vertical and radial swelling pressure indicated swelling anisotropy. Transient measurement of relative humidity and water content revealed a redistribution of porosity within the sample, which was confirmed by sampling after completion of the test. Comparison with the results of the element test showed that the two test scales are comparable in similar hydraulic states. The column test is therefore suitable as a precursor to the field test and provides valuable insights into the spatially and temporally resolved hydration behaviour of a buffer material, which helps for the design of in-situ experiments, the validation of numerical models and supports the overall process understanding.

1. Introduction

The use of compacted bentonite as an engineered barrier system (EBS) in nuclear waste repositories has been investigated in the disposal concepts of several countries, see Pusch (1977) amongst many others, owing to its low hydraulic conductivity, favourable retention properties, and pronounced swelling behaviour. Upon saturation, the development of swelling pressure ensures an effective seal and the closure of voids or fractures resulting from excavation, provided that the swelling pressure is sufficiently high. For the construction of deep geological repositories, not only the safe sealing of disposal tunnels, but also the sealing of access tunnels and shafts is of great importance (Nagra, 2002). For shaft sealings, the suitability of the sandwich sealing system consisting of vertically alternating sealing and equipotential segments is being investigated (Nüesch et al., 2002; Schuhmann et al., 2009; Wieczorek et al., 2024). This system is designed to achieve uniform hydration within barriers in shafts and drifts in underground repositories by alternating sealing segments (DS) composed of bentonite and equipotential segments (ES) with higher hydraulic conductivity. For the dimensioning of the DS, the behaviour of the compacted bentonite under different hydro-mechanical load paths has to be investigated. In Germany, there are two sources of natural bentonite deposits, which are commercially distributed under the names Securisol UHP (Stephan Schmidt KG, SSKG) from the Westerwald area and Calcigel (Clariant) from Bavaria. They are currently studied as suitable materials for the DS of the sandwich system. In contrast to most studies on radioactive waste disposal, which focus on Na-bentonite, Calcigel and Securisol UHP are both Ca/Mg-bentonites (Asaad et al., 2025) whose hydration and swelling behaviour has been less extensively investigated. Therefore, this work examines the infiltration and swelling behaviour of Calcigel.

In general, the coupled (thermo-)hydro-mechanical(-chemical) ((T)HM(C)) behaviour of compacted barrier materials is investigated through experiments at different scales, ranging from small-scale laboratory tests to real scale field experiments. The former are mainly carried out at the so-called element test scale with sample geometries of the order of a few cm, having the advantage of short test durations. However, they represent a homogeneous element of material,

☆ This article is part of a Special issue entitled: 'Clay Conf. Hannover 2024' published in Applied Clay Science.

* Corresponding author.
E-mail address: antonia.nitsch@rub.de (A. Nitsch).

https://doi.org/10.1016/j.clay.2025.108067
Received 11 April 2025; Received in revised form 26 November 2025; Accepted 26 November 2025
Available online 4 December 2025

which does not allow spatially resolved observation of the material behaviour. In contrast, field experiments on a real scale provide the most realistic information on material behaviour, but their installation and instrumentation are extremely complex, expensive, and time consuming. Mock-up laboratory tests ranging from few decimetres to few metres in dimensions therefore serve as a precursor to field scale tests, enabling the spatially and temporal resolved observation of the hydro-mechanical behaviour at well defined boundary conditions with less costs and time effort. Depending on the objective, mock-up tests can either downscale in-situ experiments, referred to as semi-technical scale, or upscale element tests, in which case they represent laboratory-scale mock-up tests. Examples of documented real-scale experiments are the Full-scale Engineered Barrier Experiment (FEBEx) in the Grimsel underground research laboratory in Switzerland Enresa (2006), the Temperature Buffer Test (TBT) at the Äspö Hard Rock in Sweden (Sandén et al., 2007) or the Sealing Experiments (SEALEX) at Tournemire Underground Research Laboratory in France (Mokni and Barnichon, 2016). Therein, supporting laboratory-scale mock-up tests were conducted on the respective materials, see Martín and Barcala (2005), Akesson et al. (2009), Wang et al. (2013) and Saba et al. (2014b).

The impact of possible material inhomogeneities is of key interest for the performance of the EBS. Inhomogeneities within bentonite used in the EBS are likely due to the backfilling or installation processes in terms of density variations or due to variation of intrinsic properties in the material itself. The tendency towards homogenization of initially heterogeneous bentonite for EBS was first observed after dismantling of the in-situ Engineered Barrier (EB) experiment in Mont Terri (García-Siñeriz et al., 2008, 2015) and thereon based investigated in the laboratory within the Beacon project (bentonite mechanical evolution) by Villar et al. (2021), Bernachy-Barbe (2021), Darde et al. (2022) and Chang et al. (2023) amongst others. Several configurations of bentonite compacted to different dry densities, combinations of bentonite blocks and pellets and consideration of technical voids demonstrated that despite the tendency towards homogenization residual heterogeneity persisted, strongly influenced by the density gradients and boundary conditions (Bernachy-Barbe et al., 2020; Villar et al., 2021). Conversely, a material that was originally homogeneously compacted can become inhomogeneous in terms of its dry density as a result of hydration and swelling, which in turn can influence the subsequent material behaviour. Intrinsic inhomogeneities can have a magnifying or dampening effect. For both cases, the sealing function must be ensured. The effects of density redistribution in originally homogeneous materials cannot be evaluated in element tests and mock-up tests are required for this purpose. As demonstrated by Wang et al. (2013), Saba et al. (2014b) and Rawat et al. (2019), hydration-induced density redistribution is a commonly observed phenomenon in laboratory scale mock-up experiments.

Mock-up tests reported in the literature focus on different aspects of the repository relevant boundary conditions, such as the behaviour under temperature and/or hydraulic gradients. The test setups are equipped with appropriate measuring devices for this purpose. This typically includes the measurement of vertical stress (swelling pressure), temperature, relative humidity and pore water pressure or suction. While radial stresses are often disregarded in element-scale tests owing to the small height-to-diameter ratio, their measurement yields valuable insights into the temporal and spatial evolution of the stress state during hydration in laboratory-scale mock-up experiments. Ambiguous results have been reported for the stress ratio and evolution of the stress field, wherein influencing factors include initial dry density, compaction direction, type of bentonite-based material and sample dimensions. Lee et al. (2012), for instance, reported radial stress measurements during swelling tests on uniaxially compacted small samples (d = 50 mm, h = 30 mm) of a calcium bentonite and observed anisotropic equilibrium stress states, which became more pronounced with increasing dry density, and thus with increasing compaction energy. By contrast, Saba et al. (2014a) and Cui (2017) found that, in small samples of a bentonite–sand mixture (d = 38 mm, h = 10 mm), the stress state tended to become more isotropic with increasing dry density obtained by uniaxial compaction. In mock-up tests, investigations of isotropically compacted specimens by Akesson et al. (2009) on MX80 bentonite (d = h = 200 mm) and by Dieudonné et al. (2024) on a bentonite–sand mixture (d = 120 mm, h = 100 mm) revealed anisotropic stress fields, where radial stress partly exceeded, or at least equalled, the vertical stress. Similar results were reported for uniaxially compacted specimens by Rawat (2019) for a bentonite–sand mixture (d = 100 mm, h = 300 mm) and by Bernachy-Barbe et al. (2020) for powder–pellet mixtures of bentonite (d = 240 mm, h = 103 mm). In contrast, Saba et al. (2014b) reported lower radial stresses than vertical stresses for a bentonite–sand mixture (d = 60/120 mm, h = 120 mm). Comparable findings indicating different stress ratios and anisotropic stress states were observed in laboratory tests focusing on the influence of technological voids (see e.g. Harrington et al. (2020), Daniels et al. (2021), Bernachy-Barbe (2021) and Darde et al. (2022)). Overall, radial stress measurements in mock-up tests indicated a radial stress gradient with increasing distance from the hydration end. However, the stress ratio remains a subject of ongoing research, given the inconclusive experimental evidence. However, in most of the previously reported laboratory mock-up tests only relative humidity was measured and water content measurements were omitted due to the complexity of the measurement technique and calibration, though the migration of water inside the sample is the governing mechanism upon hydration. In the present study, both the water content and relative humidity, as well as vertical and radial stresses over the height of the column have been monitored in a column test device. This column test device was first implemented for investigation of the (thermo-)hydro-mechanical behaviour of a Calcigel–sand mixture (Rawat et al., 2019, 2021) and is here employed on compacted Calcigel granules.

In the context of the Sandwich sealing system, large scale in-situ experiments are currently performed at Mont Terri (Emmerich et al., 2019; Wieczorek et al., 2021, 2024). They are accompanied by mock-up tests at semi-technical scale, representing the sandwiched shaft sealing construction, with Calcigel and/or Securisol as the sealing material for the DS (Koeniger et al., 2008; Emmerich et al., 2009; Wieczorek et al., 2024). In the present work, the focus is on the hydro-mechanical behaviour of compacted Ca/Mg bentonite (Calcigel) granules observed in both laboratory element tests and a laboratory mock-up test on decimetric scale, hereinafter referred to as column test. This way, the hydration behaviour of the bentonite DS material is evaluated without possible influences from the layered sandwich system. The column test allows to investigate heterogeneities in swelling and hydration behaviour and investigate effects of a hydration-induced density redistribution, which is not evident on smaller scales.

The column test was carried out under ambient temperature (T = 20°C), as the hydration behaviour in the far field from the waste canisters in the deep geological repository is of interest here. The test was hydrated with deionized water from the bottom and ran for 370 days from March 2023 to March 2024. To support the design and interpretation of the decimetric laboratory mock-up test, and to gain insights into the small-scale behaviour an extensive experimental campaign on element test level was carried out, comprising constant volume swelling pressure tests and constant volume wetting paths of the soil water retention curve (SWRC).

2. Material

The investigated material is Calcigel, which is a commercially available bentonite from Bavaria, Germany. Table 1 summarizes the relevant geotechnical and mineralogical properties of the material, which were mostly determined according to DIN EN ISO standards (Deutsche Institut für Normung e.V.). Calcigel is highly expansive and classified as

Table 1
Geotechnical and mineralogical properties of Calcigel (Asaad et al., 2025).

Properties	Values
Grain density ρ_s, g/cm^3	2.738 (105°C) / 2.740 (200°C)
Liquid limit w_L, wt.%	109.8[a] / 117.2[b]
Plastic limit w_P, wt.%	33.9
Shrinkage limit w_S, wt.%	12.0
Initial water content[c] w_0, wt.%	11.9 – 13.3 (105°C) / ≈ 15±0.4 (200°C)
Plasticity index I_P, wt.%	79.0
Consistency index I_C, wt.%	1.3
Smectite content, wt.%	61 (dioctahedral)
Cation exchange capacity, cmol(+)/kg	60
Specific surface area a_s (N_2)[d], m^2/g	57
Specific surface area a_s (EGME)[e], m^2/g	460

[a] Fall cone method.
[b] Casagrande method.
[c] Equilibrium water content under ambient conditions as received.
[d] N_2-adsorption isotherms (BET-method according to Brunauer et al. (1938)) in the adsorption range of 0.04 – 0.2 p/p_0.
[e] Total specific surface area including interlayer and external surfaces, determined by adsorption of the polar molecule ethylene glycol monoethyl ether (EGME according to Carter et al. (1965) and Cerato and Lutenegger (2002)).

a highly plastic clay based on its Atterberg limits according to DIN 18196:2023-02 (2023). The predominant exchangeable cation is calcium (Ca^{2+}: 41.5±1 cmol(+)/kg), followed by magnesium (Mg^{2+}: 18.5±1 cmol(+)/kg), sodium (Na^+: 2.9 ± 1 cmol(+)/kg) and potassium (K^+: 1.0±1 cmol(+)/kg). The water content at ambient laboratory conditions corresponds to a 2W-state (2 water layers in the interlayer space). The bentonite used in this study is in the form of a granulate with a maximum granule size of 4 mm. During production, the raw material was first broken down, dried to 10 wt.% water content (105°C), milled to a size of < 500 μ m (supplier: Clariant) and subsequently compressed into pillows ($m \approx 9 - 10$ g, dim. ≈ $40x15x10$ mm^3, producer: Stephan Schmidt KG). Finally, the pillows were crushed into granulate. The apparent grain size distribution of the granulate was determined by combined dry sieving and sedimentation (DIN EN ISO 17892-4:2017-04, 2017). Characteristic percentile values of the apparent grain size distribution are d_{10} = 0.23 mm, d_{50} = 1.55 mm, and d_{90} = 3.35 mm. The apparent fines content of the granulate is 2.19 wt.% for d < 0.063 mm. Calcigel has been a subject of geotechnical research for a considerable time period. First element tests on Calcigel, formerly known and still marketed as Montigel, reach back into the 1980s, see e.g. Bucher and Spiegel (1984), Bucher and Müller-Vonmoos (1989). A large number of element tests on the material were further carried out by Agus and Schanz (2008), Baille et al. (2010) and Lang et al. (2019), which serve as reference for the results of this work. For a more detailed mineralogical characterization and geotechnical classification the interested reader is kindly referred to Asaad et al. (2025).

3. Experimental methods

3.1. Column test: experimental set-up

The column test was carried out in a sophisticated column type experimental set-up. It was first developed and described by Rawat et al. (2019) for testing of a bentonite–sand mixture, whereas in this work, the infiltration behaviour of a bentonite is investigated. The design has been slightly refined since then by modifying the head of the column to allow vertical loads to be applied using a solid screw. Although this paper only considers constant volume conditions, different mechanical boundary conditions can be considered in the future.

The layout including cross sections and a photograph of the test set-up is shown in Fig. 1. In there, a cylindrical sample with the dimensions h = 30 cm and d = 15 cm, which consisted of 3 blocks of h = 10 cm each (items 2, 3 and 4), were installed. The sample was fitted in three rings (d_{in} = 15 cm, d_{out} = 35 cm, items S1, S2 and S3) and vertically limited by a plug at bottom (item 5) and top (item 1). The rings and plugs were made of polyvinylidene fluoride (PVDF). PVDF ensured thermal insulation for the test set up as it is a non-reactive thermoplastic with a very low thermal conductivity (0.13 W/m· K) and sufficient stiffness to withstand the loads occurring during the test (Rawat, 2019). One load cell each (items 6 and 7, OMEGA Eng.: LCM-402 with capacity 100 kN and accuracy ±0.3%) was installed above and below the top and bottom plugs respectively to measure the vertical stress. A confining steel cylinder (item 8) ensured the placement of the rings and plugs. The column was constrained by a rigid frame serving as counter bearing (item 9). The vertical loading screw (item 17) was fixed during the infiltration test to ensure constant volume conditions.

Top and bottom of the sample were in contact with stainless steel porous plates (d = 15 cm, h = 1 cm) at the inner end of the plugs. These further consisted of an intermediate piston for load transfer (d = 14.8 cm, h = 10 cm) and a stainless steel cover at the interface with the load cell (d = 15 cm, h = 20 cm). To prevent the top and bottom plugs from tilting or shifting, they were also enclosed in rings in the same way as the soil sample.

For hydration, water was supplied to the sample through water inlets in the top and bottom plugs with help of an additional air vent (item 13) and an infiltration burette with a low pressure of approximately 1 mH_2O ≈ 0.1 bar. To prevent evaporation, the burette was covered with a lid. The measurement accuracy was 0.1 ml. The water level in the burette was monitored and read frequently at the beginning of the test and then at longer intervals as the test progressed, first daily and later weekly. The top and bottom plugs further included temperature control coils (items 16) connected to a thermostat, through which the test set-up was heated or cooled by circulating tempered silicone oil. The target temperature of 20°C was ensured by the external thermostat (indicated with red arrows in Fig. 1, (Huber CC-202 with range 20°C to 95°C and stability = ±0.02°C) connected to a temperature sensor (Pt100) installed in the head section as a reference temperature for the external thermostat.

In addition to ensuring the oedometric constraint and thermal insulation, the sample rings along the sample contained the entry ports of the measurement sensors in the three horizontal measurement sections located each at midheight of the respective block. They are referred to as 'top', 'mid', 'bottom' at 5 cm, 15 cm and 25 cm distance from the infiltration site at the bottom sample end, respectively (see Fig. 1 c). The measuring equipment of the column includes the following sensor types, each positioned at a quarter of the circular horizontal cross-section of the column. They are (1) load cells for radial stress measurement (item 10, OMEGA Eng.: LCM-203 with capacity 5 kN and accuracy of ±0.3%), (2) time domain reflectometry sensors (TDR) for water content measurement (item 11, IMKO PICO-32; measurement range 0 to 70% with accuracy ±2% for 0%–40%, ±3% for 40%–70%), (3) Pt100 sensors for temperature measurement (item 14, d = 3 mm, l = 150 mm, l ≈ 10 mm embedded in sample; measurement range −40°C to 200°C with accuracy (0.1 + 0.0017 × $|T|$)°C and (4) relative humidity (RH) sensors (item 15, VAISALA HMT337 with heating option and additional Pt100 probe embedded (as above); measurement range for relative humidity of 0−100% RH with accuracy of ±1% RH (0−90% RH) and ±1.7% RH (90−100% RH) for the temperature range of 15−25° C applicable for the column test. Each sensor was inserted into a special adapter made of PVDF, which was screwed into the sample rings and sealed with O-rings preventing loss in humidity and temperature. For the insertion of the TDR and Pt100 sensors, holes were drilled radially into the sample, as indicated in the horizontal cross-section in Figure Fig. 1 a. For the radial load cells, a counter bearing was installed at the outside of the confining cell. Between the bottom and mid block and the mid and top block, two earth pressure transducers (item 12, KYOWA-BEC with capacity 1 MPa and accuracy ±0.03 MPa) were installed for additional vertical stress measurement. Their cables were routed out via the Pt100 sensor adapters at the mid and top section. Appropriate recesses were cut into the sample for correct positioning of the sensors upon sample preparation.

Further details about the construction of the column and the monitoring sensors including manufacturer and measuring range are given in Rawat et al. (2021).

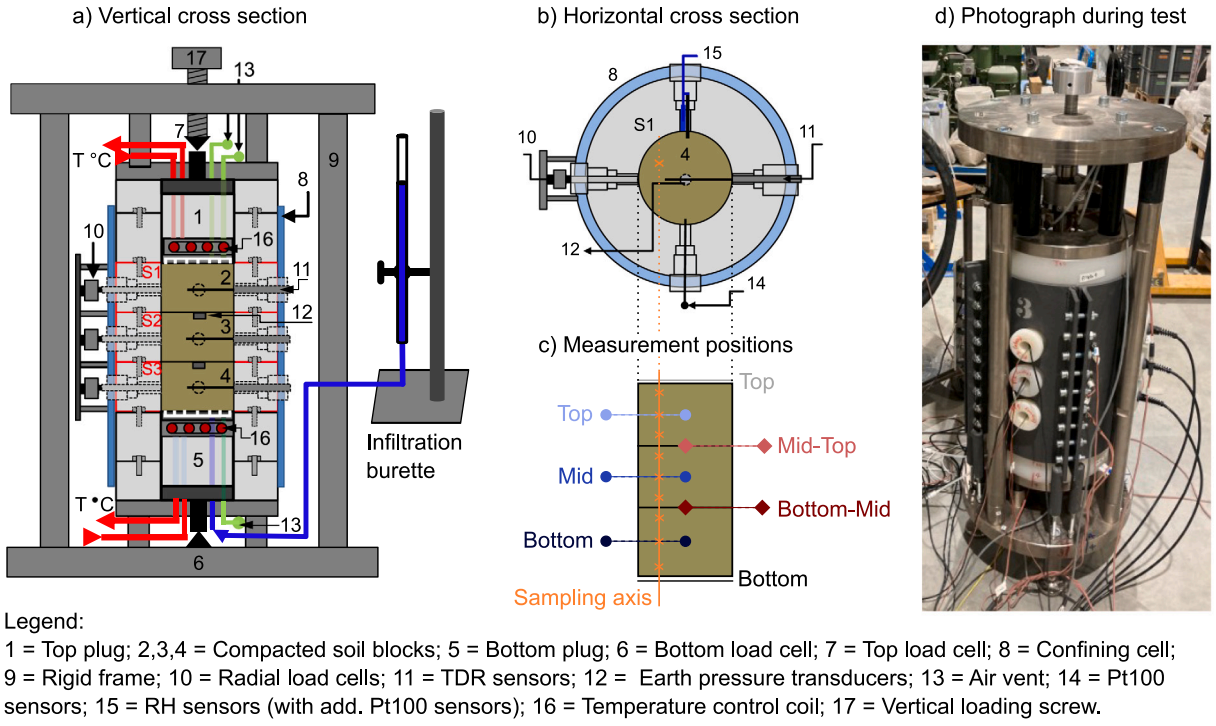

Fig. 1. Layout of the column type test device: vertical cross section (a), horizontal cross section (b), measurement positions (c) and photograph (d). Based on (Rawat et al., 2019).

3.2. Column test: calibration of TDR-sensors

The time-domain-reflectometry (TDR) technique uses the correlation between the transit time of electromagnetic waves and the real part of the dielectric permittivity of the medium surrounding the TDR-sensor. Since the dielectric permittivity of water is much higher than that of soil solids and air, it is used as indicator for the volumetric water content of the soil. Thus, the measured transit time of the initial pulse in the sensor until receiving its reflection is related with the volumetric water content of the surrounding soil. Initially, the functionality and accuracy of each TDR-sensor was verified using a defined volume of glass beads with either air-filled or water-saturated pore space. Subsequently, a material specific two-step calibration procedure of each TDR-sensor was carried out. For this, separate Calcigel sample blocks at four different known water contents were compacted at identical target dry density of 1.55 g/cm^3. Subsequently, each TDR-sensor was inserted into the blocks and its output signal in terms of travel time t_p was measured in each Calcigel block at known gravimetric water contents for room temperature of 20°C. The travelling time of the sensors was measured at a signal frequency of 1 GHz and during a duration of approximately 1 min and was averaged over the measurement time. This calibration procedure was repeated after stepwise heating to different temperatures between 20°C and 80°C, while the gravimetric water content was kept constant by sealing of the sample blocks. The water loss was found to be minimal by comparing the final measured gravimetric water content (using oven drying method) after the final heating step to the initial preparation water content. For each sensor, the established calibration curves in terms of measured travelling time t_p in ps against gravimetric water content were linear, but unique for each temperature T. The water content was evaluated by linear interpolation in the $t_p - w - T$ space. It is to be noted that these calibrations are valid for the given dry density of 1.55 g/cm^3. Therefore, in a second step after the test, the measured water contents using the above established calibration relation were scaled by the final gravimetric water content values measured by oven drying in the postmortem sampling (see following section). An example of the calibration curves is given in supplementary material.

3.3. Column test: sample preparation and testing procedure

Three blocks of compacted Calcigel were prepared for the test by vertical compaction in a steel mould in an uniaxial static compaction device. Necessary sensor and cables recesses were prepared. The first block was carefully pressed by hand into the PVDF ring previously mounted on the base of the column test-device. Few gaps around cables and the inner earth pressure sensors were filled with finely ground bentonite to avoid water leakage. The top surface of the block was scarified to ensure optimal contact with the adjacent upper block. These steps were repeated for the second (mid) and the third (top) block. Subsequently, the top plug with porous stone, the confining cell, all sensors and the counter bearing for the radial load cell were installed. The rigid frame was mounted in the last step and the vertical loading screw was tightened while monitoring the load cells for vertical stress until sufficient contact was established ensuring the constant volume conditions of the test. Finally, the water supply, thermostats and measurement acquisition system were connected.

The infiltration test was conducted at a target temperature of 20°C controlled by the thermostats at the top and bottom plug. The sample was infiltrated from the bottom, while the upper air vent was open for air to evacuate. The test ran for a period of 370 days during which the vertical stress, radial stress, relative humidity, water content and temperature were measured at different positions of the sample. After completion of the test, the test set-up was demounted and post-experimental sampling was carried out at different locations along the height of the sample. For this, a continuous vertical measuring axis was defined inside the quarter cross section undisturbed by measuring sensors. Along this measurement axis, three small samples of each block, hence nine in total, were collected (see Figure Fig. 1 b and c). Selected samples were further taken at different horizontal distances from the centre in the undisturbed lower part of each block. Water content was determined by oven drying (105°C and 200°C) and the bulk density was measured by immersion weighing (in air and paraffin oil, see Christ et al. (2022)) using a precision scale.

Table 2
Initial ($\sqcup_0$) and final ($\sqcup_f$) conditions of the swelling pressure element tests.

Name	Vertical compaction stress σ_{prep} (MPa)	Dry density $\rho_{d0}\|\rho_{df}$ [a] (g/cm^3)	Water content $w_0\|w_f$	Degree of saturation $S_{r0}\|S_{rf}$	Swelling pressure σ_v (MPa)
Cal-Q-04	14.2	1.72 | 1.61	0.119 | 0.258	0.552 | 1.194	3.8
Cal-Q-08	–	1.63 | 1.54	0.119 | 0.290	0.477 | 1.144	2.7
Cal-Q-02	9.3	1.61 | 1.52	0.119 | 0.290	0.462 | 1.127	2.0
Cal-Q-01	8.8	1.61 | 1.52	0.119 | 0.287	0.464 | 1.119	1.7
Cal-Q-07	–	1.52 | 1.43	0.119 | 0.340	0.406 | 1.148	0.8
Cal-Q-11	6.6	1.53 | 1.46	0.133 | 0.314	0.465 | 1.091	1.0
Cal-Q-10	7.0	1.55 | 1.52	0.133 | 0.297	0.477 | 1.058	1.7
Cal-Q-09	7.7	1.57 | 1.53	0.119 | 0.294	0.489 | 1.074	1.9
Cal-Q-03	7.1	1.45 | 1.37	0.119 | 0.380	0.376 | 1.198	0.6
Cal-Q-06	5.3	1.42 | 1.36	0.119 | 0.376	0.349 | 1.103	0.4
Cal-Q-05	4.7	1.26 | 1.22	0.119 | 0.449	0.276 | 1.042	0.1

[a] The final dry densities were determined by measuring the heights of the samples within their oedometric rings after removing the vertical restraint of the constant-volume test set-up.

3.4. Element tests: methods and sample preparation

The element tests, which serve for evaluation of the column test results, include swelling pressure tests and determination of the soil water retention curve at constant volume conditions. For both test types, the samples were prepared by uniaxial static compaction. Swelling pressure tests were conducted on oedometric samples (d = 5 cm, h = 2 cm) in constant volume isochoric cells (Romero, 1999; Schanz and Tripathy, 2009; Agus et al., 2013), wherein analogously to the column test, infiltration was realized with a burette from the bottom and water was distributed by porous stones. An upper air outlet prevented pressure build-up in the cell. Swelling pressure was measured as a reaction force with a load cell mounted in the top of the cell and transferred via the cross section of the sample. The load cell had a capacity of maximum 22 kN, which corresponds to approximately 11 MPa for the specimen diameter d = 5 cm.

The soil water retention curve (SWRC) was determined by subjecting the initially compacted samples with initial suction of about 71 – 74 MPa, initial water content of about 12 wt.% and being constrained in a constant volume microcell (d = 30 mm, h = 7 mm, Seiphoori et al. (2014)) to a total suction of about 2 MPa using the vapour-equilibrium (VET) technique. In regular time intervals, the water content was measured by weighing and the corresponding suction was measured by chilled-mirror hygrometer (AquaLab CX-3TE d by METER Group Inc). The microcells allowed hydration of a previously compacted sample through perforations in their outer walls by simultaneously maintaining constant volume conditions. They were designed to fit into the chamber of the chilled-mirror hygrometer, which determined the relative humidity by measuring the dew point temperature at which condensation of the sample clouds the chilled mirror of the device at controlled temperature (Leong et al., 2003).

3.5. Test program

For the column test, the target dry density was chosen as ρ_{d0} = 1.55 g/cm^3, as it corresponds to the initial condition in the Sandwich Main Project in-situ experiment (Wieczorek et al., 2024). Note that this value, as well as all following dry densities and water contents, correspond to oven-drying at 105°C. At this temperature, not all structural water of bentonite is yet accounted for, however in geotechnical engineering it is the standard practice and thus applied in this work. Upon preparation, the material was uniaxially compacted to the desired height of h = 10 cm for each block. To avoid density gradients, a procedure developed by Rawat (2019) for the compaction equipment was followed: the material was placed in layers into the compaction mould, after the inner surfaces of the mould had been lubricated using Teflon spray. Each layer was only lightly pressed, well below the final expected compaction stress and the surface was roughened before adding further material. Finally, the complete target mass of the material was compacted to the final height of the sample block. A vertical compaction stress of $\sigma_{prep} \approx 6$ MPa was recorded at the end of the compaction stage. This procedure has proven effective in achieving a nearly homogeneous density inside a block (Rawat, 2019). However, a non-destructive verification of the as achieved distribution of the densities in the column test blocks could not be performed. The achieved dry density ρ_{d0} = 1.54 g/cm^3 of each of the three blocks showed a good reproducibility of the initial target dry density of 1.55 g/cm^3. With an initial water content of w_0 = 0.128, the initial degree of saturation and initial suction were S_{r0} = 0.456 and s_0 = 66 MPa respectively.

A whole experimental swelling pressure element test campaign was realized prior to the column test with a range of dry densities from ρ_{d0} = 1.25 – 1.73 g/cm^3 including four replicate tests (samples Cal-Q-07, -09, -10 and -11) with similar densities as the column test samples for sake of comparison. Table 2 provides an overview of the initial conditions regarding compaction pressure, dry density, water content and degree of saturation of the swelling pressure element tests. At the given dry density, the required vertical pressures during static compaction as measured by a load cell in the compaction device were slightly larger compared to those for the column test samples due to different sample dimensions. However, the intrinsic pre-compaction pressure of the compacted samples corresponding to a specific dry density is thus in a very similar range for both the element tests and the column test. For the soil water retention behaviour during wetting at constant volume condition, five data series covering the initial dry densities of $\rho_{d0} = \{1.27, 1.41, 1.50, 1.61, 1.72\}$ g/cm^3 were obtained. The initial water content was at w_0 = 0.119 for all samples.

4. Experimental results

4.1. Element test results: swelling pressure and SWRC

In Fig. 2a, the evolution of swelling pressure measured in eleven element tests is shown. In all tests, swelling pressure increased rapidly after the start of infiltration, reaching a first equilibrium after 3–4 days, before rising with a smaller gradient to a final equilibrium value after approx. 15 days. This characteristic transient behaviour is typical for element tests on bentonite and attributed to an internal redistribution of pore space in the microstructure of the compacted material upon saturation. The equilibrium swelling pressures showed a logical dependency on the initial dry density and ranged between $\sigma \approx 0.1 - 3.8$ MPa for the presented dry density range. The final conditions of the swelling pressure tests on element scale are gathered in Table 2. The final dry densities refer to the state after removing the vertical displacement constraint within the constant-volume test set-up, thus including elastic unloading in the fully saturated state. The final degree of saturation was calculated with the initial dry density, which corresponds to the constant-volume conditions during saturation. The calculated final degrees of saturation exceed a value of 1, as the assumed water density of

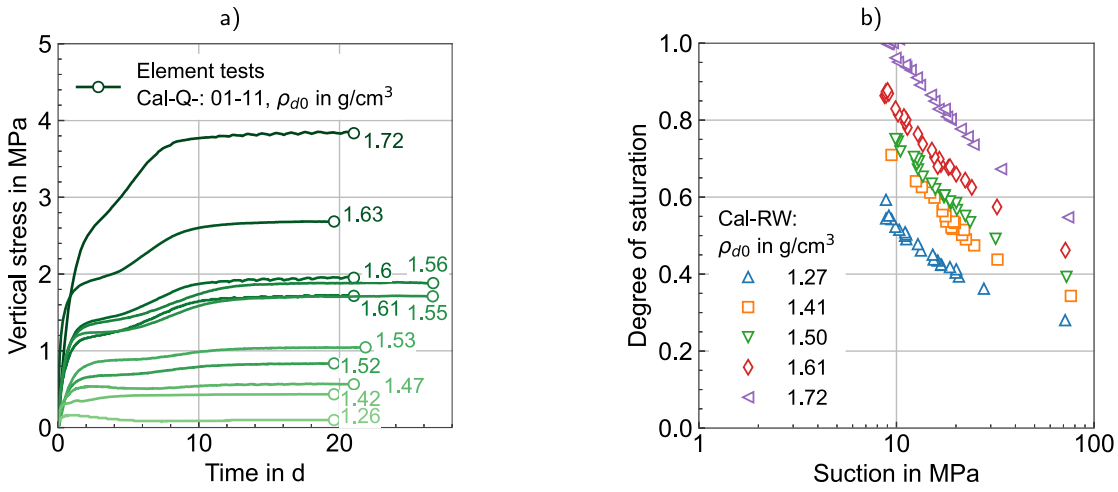

Fig. 2. Results from element tests: a) vertical stress vs. time from constant volume swelling pressure tests b) wetting soil water retention curve at constant volume in terms of degree of saturation vs. suction.

$\rho_w = 1.0$ g/cm^3 does not account for the higher actual water density in bentonites and S_r is thus overestimated. Studies of Jacinto et al. (2012), Navarro et al. (2022) and Wang (2024) amongst others have shown that water density increases with decreasing suction and with increasing dry density of bentonite. This trend is reflected in the final values reported in Table 2, where, aside from individual outliers, higher initial dry densities overall corresponded to higher final degrees of saturation.

The water retention behaviour is presented in Fig. 2b in terms of degree of saturation versus suction for five test series. The initial suction and water content were very similar. A pronounced dependency of the retention behaviour on the dry density became apparent in the S_r–log(s) space: for a given suction, an increased degree of saturation was observed with increasing dry density of the samples due to the overall reduction in available pore space. For the water content, less pronounced differences than for the degree of saturation were evident and the five test series coincided in a bandwidth in the w–log s space. The final water contents of the samples showed only a slight difference of $\Delta w_{\max} \approx 3\%$ between the loosest and densest sample.

4.2. Column test results: time evolution

All plots in Figs. 3 and 4 show both the raw signal (light line) and the smoothed signal (dark line) for each measurement section. The smoothed data were obtained using a Savitzky–Golay filter (polynomial fit that preserves signal shape and peaks).

In Fig. 3a the evolution of relative humidity over time is shown for the three measurement sections ('bottom', 'mid', 'top' at 5 cm, 15 cm, 25 cm distance from the infiltration site, respectively). A very sharp and direct increase was observed in the bottom measurement section, which reached a RH value of 95% already after 80 days followed by only a small increase up to 96% until the end of the test. In the mid and bottom section the relative humidity increased more steady after an initial delay of about 10 to 20 days. In the mid section, RH increased asymptotically towards the final value of the bottom section, while the RH in the top section showed a continuous increase over the whole test duration. After 370 days the final measured RH values were 96%, 94% and 84% from bottom to top.

The evolution of water content over time is presented in Fig. 3b. Therein, the initial water content (w_0) and the calculated maximum water content ($w_{\max}$) assuming fully saturated state ($S_{r,\text{sat}} = 1.0$) and ideal constant volume condition during hydration (dashed horizontal lines) are shown. In general, the raw TDR sensor signal was more scattered than the RH signal. Moreover, after a continuous increase during the first 105 days, the bottom sensor displayed strong oscillations, which were not observed in the mid and top sections. Possible reasons for the oscillations are the following: (1) the TDR measurement is not a point measurement, but represents the water content of a cylindrical soil volume (5 cm diameter, 11 cm length) around the sensor axis. Thus, the TDR signal is influenced by gradients in the hydraulic state parameters inside the measurement region. (2) The dry density decreased in the bottom section due to its hydration and subsequent swelling. (3) The measured TDR signal is mainly controlled by the dielectric constant K_a of the pore water. The dielectric constant of bound water is known to be significantly smaller than that of free water at identical measuring frequency (Skierucha, 2009; Schanz et al., 2011) and to increase with increasing amount of water molecules in specific control volume of the smectite's atomic structure (Emmerich et al., 2015). The initial state with $w = 12$ wt.% corresponds to 2W-hydration state with bound water in the smectite fraction of the bentonite. With increasing water content the hydration state is expected to increase, accompanied by a change from strongly bound water molecules towards a water network approaching that of free water and a corresponding change in dielectric permittivity of the water at a given frequency. Overall, two competing mechanisms affecting the TDR-signal in the bottom block can be identified: (1) the increasing hydration towards free water state corresponding to a high dielectric permittivity, and (2) the swelling of the smectite with re-distribution of water into the interlayer pores resulting in bound water state with lower dielectric permittivity. The oscillations did not represent the real water content, however, their maxima and minima followed the same trend. Therefore, the trend of the minima was used for the water content evaluation from the time the oscillations occurred first, which was confirmed by the measured water content using oven drying at 105°C after dismantling the sample. After one year of test duration the final values reached were 28%, 20% and 17% at bottom, mid and top section respectively.

In general, the time evolution of measured water content was different from the relative humidity measurements in the respective sections. Although for both parameters a pronounced increase occurred in the bottom section, the water content still showed an increasing trend at the end of the test after 370 days. The rate of increase in water content was significantly lower in the mid section, where it developed linearly at a similar rate throughout the duration of the test. The water content increase in the top section was found to be negligible during the first 50 days and evolved between 50 days and 200 days at a similar rate as in the mid section. It should be noted that the increase rate of water content was equal in the three sections between 100 and 200 days, while, after 200 days, the water content continued to increase in the bottom and mid section at a similar rate, while the water uptake slowed in the top section. While the relative humidity for the mid section reached close to the equilibrium RH value of the bottom section of

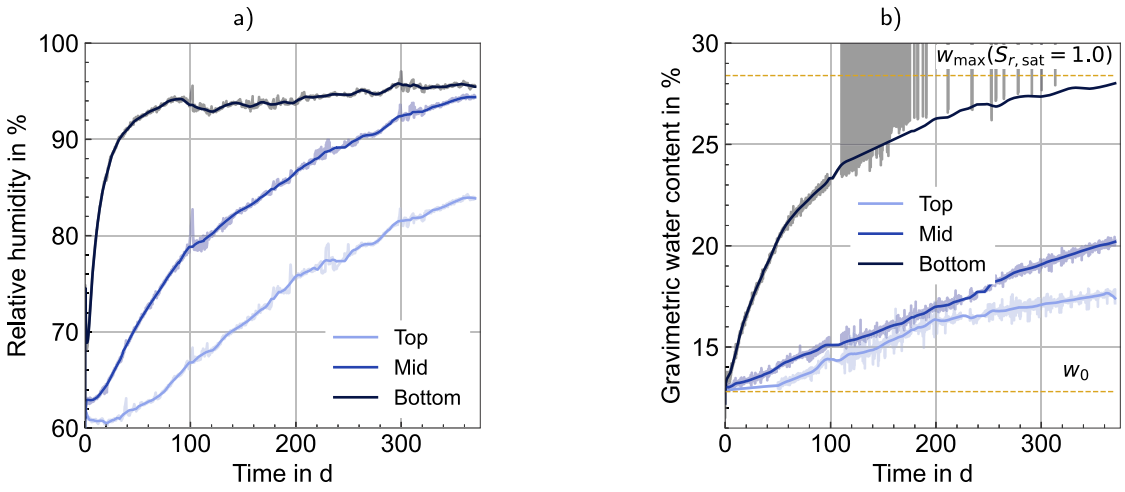

Fig. 3. Evolution of measured relative humidity (a) and gravimetric water content (b) vs. time at three measurement sections of the column test. Dashed horizontal lines in (b) indicate initial water content w_0 and the calculated water content assuming full water saturation ($S_{r0} = 1.0$) for the initial average dry density of 1.540 g/cm^3.

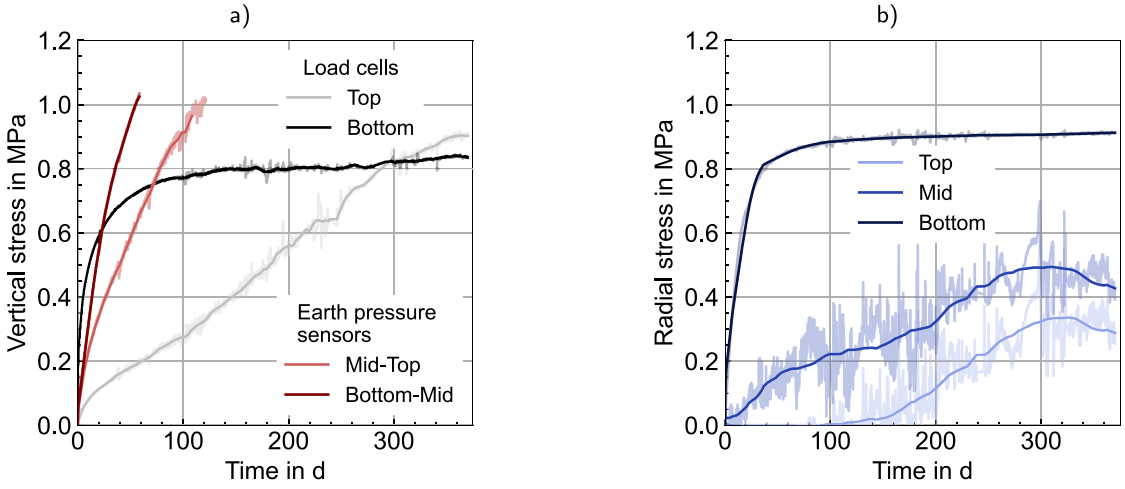

Fig. 4. Evolution of measured vertical stress vs. time (a) at the top and bottom load cell and earth pressure transducers at two heights of the column test and measured radial stress vs. time (b) at three measurement sections of the column test.

≈ 95%, the water content of the mid section did remain significantly below that of the bottom section during the duration of the test.

From relative humidity measurements, suction s was derived using Kelvin's equation. The sample temperature was slightly influenced by annual temperature changes in the laboratory hall, despite the applied temperature control in the top and bottom plug at $T = 20$°C. The fluctuations remained between $T = 18 - 21$°C and were rated as non-critical for the overall test, but do explain momentary fluctuations in the state variables.

The evolution of temperature and suction are given in supplementary material. The latter behaved reciprocally to the relative humidity, so, suction reached equilibrium in the bottom section, while it was still decreasing in the mid and top section. After one year of test duration, the final values were found to be approximately 6 MPa, 8 MPa, and 24 MPa in the bottom, mid, and top sections, respectively. The evolution of vertical stress over time is shown in Fig. 4a. In the bottom load cell, an immediate and pronounced increase in vertical stress was measured after the start of hydration. In the top load cell a significantly slower vertical stress increase was apparent. In the earth pressure sensors, where stress was measured within the sample between the bottom and mid block and the mid and top block, the stress also increased immediately after the start of infiltration and reached values higher than those of the outside load cells very quickly. As the maximum capacity of the earth pressure transducers was 1 MPa, no further measurement was possible beyond this stress level. At the end of the test, the stresses of the top and bottom load cell were similar, but still with a slight increase in tendency. The rate of swelling pressure increase was higher for the top, as the sample was less close to saturation there. The final values of vertical stress were 0.8 MPa and 0.9 MPa at the bottom and top load cell, respectively. The difference between the two measured values exceeds the accuracy of the load cell, thus, indicates a real difference in final stress state. An increased equilibrium swelling pressure is to be expected for full saturation of the sample due to more developed swelling in comparison to partial saturation, which applies for the final state of the column test.

Fig. 4 b) displays the evolution of radial stresses. Radial stress was measured at the circumference of the sample by contact with the constrained load cell (see item 10 in Fig. 1) with a rigid piston. In the bottom section, the radial stress developed was almost identical to the vertical stress, reaching a slightly higher final value. In the mid section, the radial stress also increased shortly after infiltration, while in the top it only started to increase after around 100 days. Larger fluctuations in the radial stress measurement resulting from slight temperature fluctuations affecting the steel counter-bearing were observed in the mid and top section, whereas the load cell for the radial stress measurement in the bottom section was found to be less sensitive

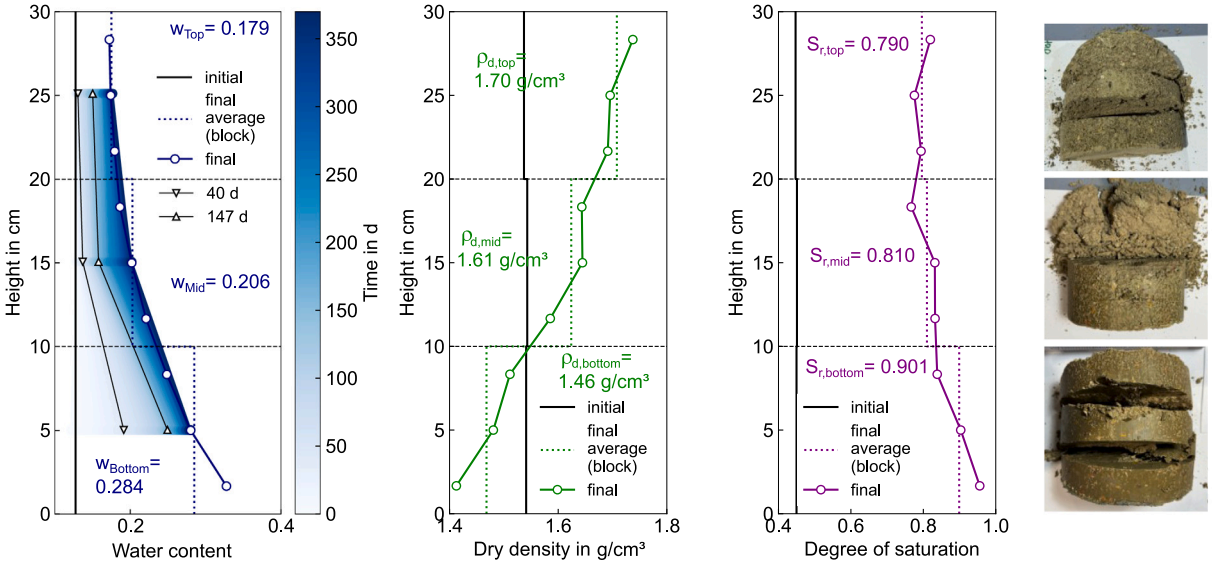

Fig. 5. Final distribution of water content, dry density and degree of saturation over the height of the sample in the column test including average value for each block, initial values for reference and water content isochrones for the duration of the test (left) and visual impressions from dismantling of the sample (right).

to temperature fluctuations due to the pronounced swelling pressure in the bottom section. The final values of radial stress were 1.0 MPa, 0.4 MPa, and 0.3 MPa from bottom to top after one year of test duration.

4.3. Post-experimental sampling of column test

After 370 days the test was terminated and the bentonite sample was dismantled from the test device. Therefore the rings including the blocks were demounted and separated from each other by manual lifting and the block height was measured. The three blocks of the soil column were found to be well bonded due to hydration and the stresses developed but still separable without applying force. Any preferred pathways were not visible at the boundaries of the blocks. Afterwards the blocks were carefully extruded from the rings by application of static uniaxial pressure. For post-experimental sampling, each extruded block was first cut in half with a handsaw and scalpel. Half was used to determine the average water content of the respective block by oven-drying. The other half was horizontally cut into three levels from which sub-samples were carefully cut out for location-dependent measurements of water content and dry density.

Fig. 5 shows the final values of water content, dry density and degree of saturation as obtained from the sub-samples distributed over the total sample height in the vertical sampling axis indicated in Fig. 1c. The initial values are presented as well for sake of comparison. The average state of each block is shown in dotted lines and numerical values. For dry density, the average value of each block was also applied to calculate the average degree of saturation.

The radially distributed measurements (not shown) at the three sections did not reveal any gradient in water content or dry density. This confirmed that the hydration process occurred as one-dimensional process, where the column design and bentonite swelling hindered any moisture loss in radial direction. The average value of each block for the dry density reveals a slight relaxation of the blocks due to sample deinstallation. The degree of saturation was calculated using the dry density determined from the sub-samples. For the water content, the isochrones derived from TDR measurements were added in Fig. 5, with two intermediate times (40 d, 147 d) highlighted.

Fig. 5 demonstrated a pronounced higher water content, corresponding to nearly fully saturated conditions close to the hydration end, which decreased rapidly over the height of the column. Only a small water content gradient existed in the upper third of the sample. The dry density exhibited an inverse trend with the lowest and highest dry density at the bottom and the top of the column, respectively. The gradient in dry density was approximately bi-linear with the change in slope at about half the sample height (15 cm).

Comparing initial and final dry density, an expansion was observed in the lower 10 cm, whereas a compaction was observed in the upper 20 cm of the column. The expansion of the bottom block led to a localized increase in pore space, allowing a greater absolute volume of water to accumulate in this region. This accounted for the observed differences in water content and relative humidity between the bottom and middle blocks in Fig. 3. However, as the water content increase in the bottom third was not compensated by the dry density decrease, a slight gradient in degree of saturation occurred in the lower third of the sample, but an almost constant degree of saturation was observed in the mid and the top block.

Photographs of the dismantled sample blocks are included in Fig. 5. A visual inspection of the material revealed that it had become wetter, resulting in a more plastic consistency and more homogeneous state from the top down to the bottom. When the top block was disassembled, the individual granules were still discernable; the material exhibited brittle behaviour and the water appeared to be contained within the granules rather than in the pore space between them. The material in the mid block showed a more plastic consistency and the individual granules were already difficult to identify. In the bottom block the material was noticeably moist, plastic and individual granules were hardly visible. There, the material appeared to be of very plastic consistency and could be cut rather than broken.

5. Discussion

5.1. Hydraulic behaviour in the column test

5.1.1. Evolution of global and local water infiltration volume

The water content measurements by the TDR sensors were evaluated volumetrically for comparison with the infiltrated water volume known from burette readings. First, the average mean value of water content $w_{av,\mathrm{TDR}}$ of the three sections was calculated and the corresponding global average degree of saturation $S_{r,av}$ was evaluated using Eq. (1):

$$S_{r,av} = \frac{w_{av,\mathrm{TDR}} \cdot \rho_s}{e} \tag{1}$$

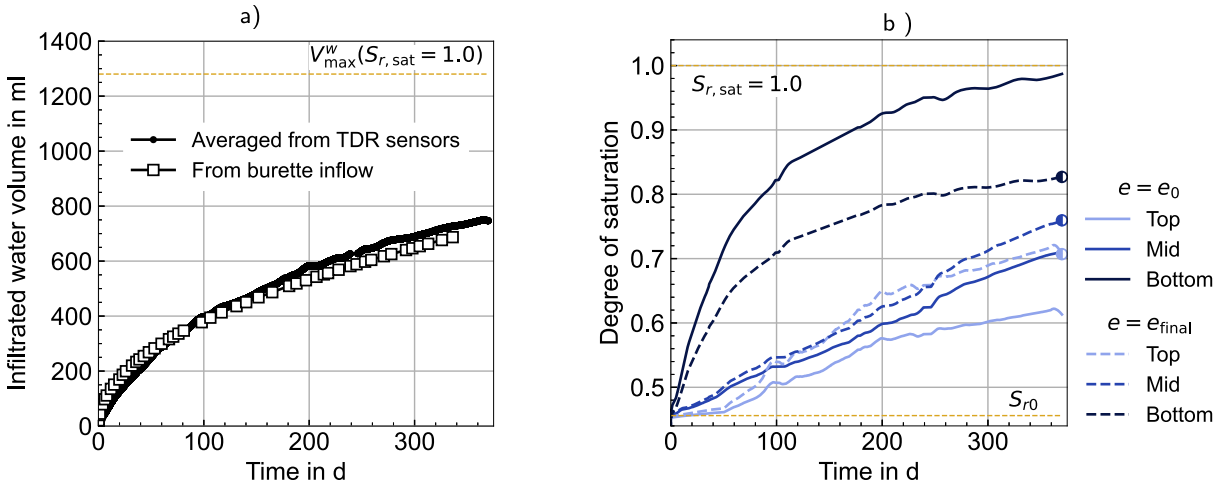

Fig. 6. Volumetric assessment of water content measurements: Comparison of infiltrated water volume from time domain reflectometry measurements and burette inflow vs. time (a) and evolution of degree of saturation vs. time at three measurement sections of the column test, calculated from time domain reflectometry measurements with assumption of constant void ratio $e = e_0$ and $e = e_{final}$ (b).

The initial average void ratio $e = e_0 = 0.766$ of the three blocks was used in the calculations, since the volume of the whole column sample remained constant, irrespective of the internal void ratio redistribution. In a second step, the total infiltrated water volume $V_{w,inflow}$ was computed using $S_{r,av}$ using Eq. (2):

$$S_{r,av} = \frac{V_w}{V_p} = \frac{V_{w0} + V_{w,inflow}}{V_p} \Leftrightarrow V_{w,inflow} = S_{r,av} \cdot V_p - V_{w0}. \quad (2)$$

Therein, V_{w0} is the initial water volume corresponding to the initial water content w_0 and V_p is the pore volume. Comparison to directly measured infiltrated water volume by the inflow burette readings (Fig. 6a) showed an excellent agreement over the whole test duration, which confirms the suitability of water content measurements by the TDR sensors.

As there was no monitoring of the local dry density changes during hydration, the real evolution of degree of saturation in each measurement section was not known, only the initial and the final void ratio were measured. Postmortem measurements after dismantling evidenced a decrease in dry density in the lower third of the sample and an increase in dry density in the upper two thirds of the sample. Therefore, the evolution of degree of saturation was done (1) using the initial void ratio e_0 in each section, which was nearly identical, and (2) the final void ratio e_f. Using e_0 overestimated the final value of S_r in the bottom section, while it underestimated S_r in the upper two thirds of the sample (Fig. 6b). Using the respective final void ratio e_{final} for each section to compute S_r, the evolution was scaled to the measured final void ratio. The two different evolutions for each section can be regarded as limiting states, where the transient evolution of the shift from the initially representative e_0-line towards the e_{final}-line being representative for large test duration could be evaluated from the measured data.

For further evaluation, the transient hydraulic gradient i was computed for the three measurement sections. Utilizing the suction computed from the measured relative humidity in the respective sections and considering the applied hydraulic pressure of $p = 10$ kPa $= 1$ mH_2O at the bottom end of the sample, the hydraulic gradient i at the distance Δl between the respective sensor position and the infiltration site at bottom of the sample is:

$$i = \frac{\Delta h}{\Delta l} = \frac{\frac{s}{g \cdot \rho_w} - 1}{\Delta l}, \quad (3)$$

wherein $g = 9.81$ m/s^2 is the gravity and $\rho_w = 1000$ kg/m^3 is the water density. In the bottom, the hydraulic gradient $i_{bottom} = 12.6 \cdot 10^{-4}$ m/m was initially largest and decreased rapidly due to the sudden presence of water after the start of hydration and the resulting flow of water. In the mid and top section located at larger height, the hydraulic gradients $i_{mid} = 4.4 \cdot 10^{-4}$ m/m and $i_{top} = 2.8 \cdot 10^{-4}$ m/m were smaller and decreased more slowly. After approximately 100 days the hydraulic gradient was equal in the whole sample at a value of $i \approx 2 \cdot 10^{-4}$ m/m and decreased further with an similar rate in all three sections, being aligned with similar rates of water content increase for the three sections after about 100 days (Fig. 3a). The decrease in average hydraulic gradient is one of the reasons attributed to the decrease in average infiltration rate after about 100 d. The evolution of the hydraulic gradient is given in supplementary material.

5.1.2. *Effect of internal pore space redistribution*

Figs. 3a and b showed that the relative humidity in mid section approaches that of the bottom section in the final stages of the test, whereas the evolution of water content at mid section is closer to that of the top section and did not approach the values of the bottom section. The different evolution of relative humidity and water content (Figs. 3a and b) in each section indicated a redistribution of the pore space, which was also evidenced by the postmortem measurements of dry density distributed over column height (Fig. 5). Porosity redistribution during hydration, where the amount of macro (interaggregate) pores reduces on account of smaller micro (interlayer and interparticle) pores within a certain constant global control volume of an element test is a well known phenomenon in expansive soils, see Delage et al. (2010), Monroy et al. (2010), Romero et al. (2011), Seiphoori et al. (2014), Wu et al. (2024) amongst many others. In mock-up tests, however, redistribution of global porosity occur due to the larger dimensions of the tests (Rawat, 2019; Akesson et al., 2009; Saba et al., 2014b). In a recent study, Dieudonné et al. (2024) conducted numerical simulations of a decimetric laboratory mock-up test and showed that the magnitude of dry density change (dry density increase in the upper part and dry density decrease in the lower part) even reached a temporary maximum and subsequently re-decreased towards the final state at saturation of the entire sample. However, the dry density change was not recovered back to the initial homogeneous state, but a dry density gradient prevailed after full saturation was reached at the end of the test. In the present study, the measured dry density gradient at the end of the test evidenced that the hydration and swelling pressure development in the bottom section was accompanied by a volume increase, where the swelling pressure exerted by the bottom section induced the compression, thus dry density increase, in the mid and top section. Both the internal redistribution in pore volume with an increase in micropore volume (interlayer and interparticle pores) on

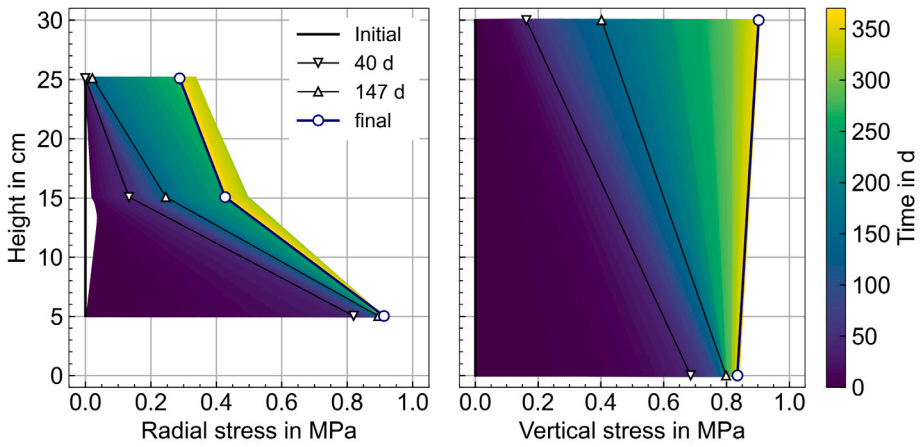

Fig. 7. Stress isochrones: Radial and vertical stress evolution over the height of the column during the whole test duration.

account of macropore volume (interaggregate pores) and the increase in dry density in the top block resulting in less available pore space for water uptake are further decreasing the water infiltration rate, as reflected by the less steep water content increase after 200 d in the top section (Fig. 3b).

5.2. Swelling behaviour in column test

Fig. 4 presents the inhomogeneous evolution of the locally varying vertical and radial stresses. In most previously reported laboratory mock-up tests, only a single vertical stress measurement was performed on one end of the sample, which was idealized as the reaction force reflecting the overall sample behaviour regardless of the position of the load cell for constant volume conditions. In this work, the two outer total stress measurements at the bottom and top end of the sample revealed distinct different evolution over time and the embedded earth pressure transducers ('bottom-mid' and 'mid-top') reached higher total stresses during their measurement time, as compared to the external measured vertical total stresses at top and bottom (Fig. 4a). At initial test stage, the hydration induced swelling pressure is mainly reflected in the bottom load cell only, whereas the other vertical stress sensors at bottom-mid section, mid-top section and top end reflect the transferred load by compression stresses. Due to friction and the dissipating effect of compressive deformation of the mid and top block, the rate of total stress increase in 'bottom-mid', 'mid-top' section and top end decreased with increasing distance from the infiltration front. With increasing time, thus, proceeding infiltration front, those stress sensors also reflect the local swelling pressure induced by hydration in the vicinity of the respective stress sensor. The continuous increase of vertical stress at the top end, exceeding the stress at the bottom end, is attributed to the increased dry density in the top section. In other words, the linear increase in the 'mid-top', 'bottom-mid' and top section are mainly controlled by the elastic loading from the expanding lower parts of the sample, whereas the steep initial total stress increase at the bottom indicated swelling in the elastic domain during the first stage followed by typical yield behaviour due to suction decrease and decrease of the apparent preconsolidation stress, leading to the flattening of the measured total stress after about 100 days. The crossing lines of the total vertical stress at top and bottom indicate that the sample has not reached an equilibrium state until end of the test, which is confirmed by the continuous increasing trend in RH and water content in the top section. In the bottom section, the transient development of relative humidity, water content and vertical stress in the bottom section revealed a very similar evolution. Hence, both the lower and upper load cell primarily reflect the respective local swelling pressure evolution.

The swelling pressure in the bottom part of the sample was lower than the externally measured compaction pressure of approx. 6 MPa upon preparation of the blocks. Nonetheless, a compression of the upper part was evident in the final distribution of dry density. The compaction pressure refers to the initial state only and does not correspond to the transient internal preconsolidation pressure. During hydration within the column, the preconsolidation pressure as well as the stiffness of the material vary in time and space, and decrease with increasing saturation or decreasing suction in bentonites (Vaunat and Gens, 2005; Monroy et al., 2010; Nitsch et al., 2023). The observed density increase in the top section can be the result of deformations in the elastic reloading regime, depending on the actual preconsolidation stress in the top section and the magnitude of swelling stress acting from the bottom section.

The evolution of bottom radial stress (Fig. 4b) showed very good alignment with both the evolution of relative humidity and vertical stress in the bottom section; hence the swelling pressure developed almost isotropically in the bottom section. In the mid and top part, the radial swelling pressure only reached approx. half to third of the vertical stress. Similar observations were made by Saba et al. (2014b) on uniaxial compacted samples hydrated from the bottom. Due to the recompression of the upper sections their volumetric swelling behaviour did manifest itself preferred in the vertical direction. The stress isochrones of the radial and vertical stress over the height of the samples during the test duration are shown in Fig. 7. The inhomogeneous and anisotropic evolution of swelling pressure becomes apparent. These results are in line with those of Lee et al. (2012) and Saba et al. (2014b) with stress ratios $\sigma_h/\sigma_v < 1$, whereas (Rawat, 2019) and Dieudonné et al. (2024) reported stress ratios $\sigma_h/\sigma_v \geq 1$. Overall, the local total stress evolution in expansive soil is the result of complex load transfer mechanisms affected by several, competing processes.

5.3. Assessment of the non-equilibrium state in column test

The column sample had not reached an equilibrium state until the test end. However, to assess the plausibility of the results from the column test, they are presented together with those of the element tests in Fig. 8 for swelling pressure and water retention behaviour. At both scales, the rapid initial increase in the swelling pressures in the element

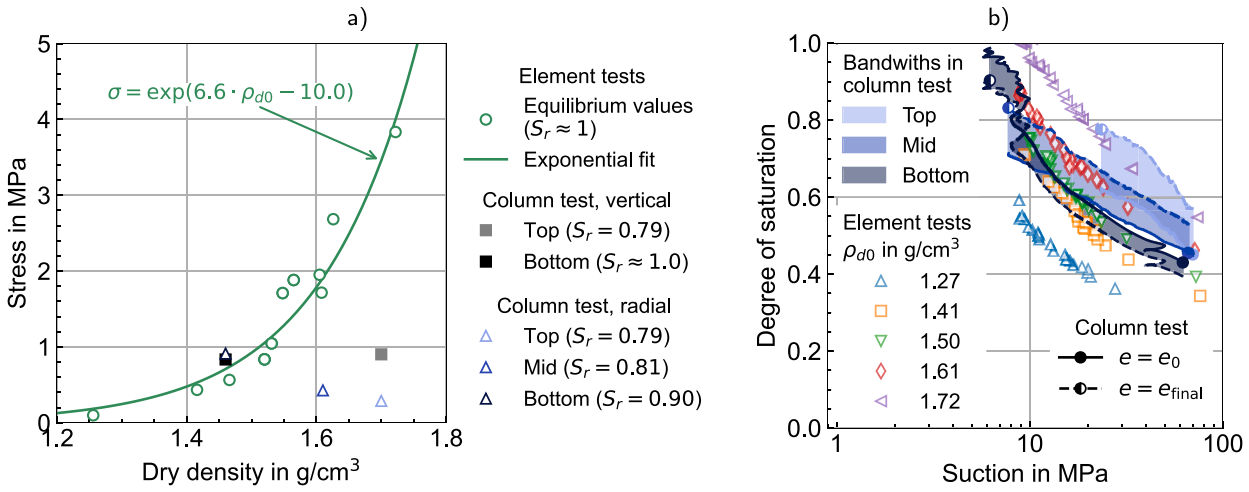

Fig. 8. Comparison of swelling pressure and wetting soil water retention behaviour in element tests and column test: vertical stress vs. dry density for the equilibrium values of the element tests and final state of the vertical and radial load cells of the column test (a) and degree of saturation vs. suction for constant volume conditions in element tests and limiting void ratios e_0 and e_{final} in column test (b).

tests and locally near the hydration end in the column test was evident (see Figs. 2a and 4a). However, the qualitative time evolution of stress observed in the element tests, with an initial equilibrium followed by a gradual increase to a final value, was not observed in the external vertical swelling stress measurements in the column. This indicates that locally occurring double structure effects caused by hydration-induced microstructural pore size evolution are masked by density redistribution at the decimetric scale of the column.

Fig. 8a directly compares the magnitude of final swelling pressure measured at different heights in the column to the equilibrium swelling pressures of the element tests as function of final dry density. In the column test, full saturation ($S_r = 1.0$) was not yet reached in all sections of the column after the test duration of 370 days, while in all element tests $S_r = 1.0$ was determined by oven-drying (at 105°C) after 20 to 27 days of hydration. The typical exponential increase in swelling pressure with increasing initial dry density was observed for the element tests, for a dry density range between $\rho_d = 1.25 - 1.73$ g/cm^3, resulting in swelling pressure between 0.1 – 3.8 MPa. The exponential equation for the final swelling pressures as a function of dry density is given as well in Fig. 8a. The magnitudes of swelling pressure were in line with prior experimental studies on Calcigel by Agus and Schanz (2008), Schanz and Tripathy (2009), Baille et al. (2010), Lang et al. (2019), Wieczorek et al. (2024). Their equilibrium swelling pressures were within the measurement accuracy with slight deviation from the overall exponential relation.

The vertical swelling pressures measured in the bottom section of the column test showed good agreement in magnitude with the element scale tests, considering its state close to full saturation. In the top section, based on the actual elevated dry density in combination with the unsaturated state, a prospective further swelling pressure increase is expected, shifting the actual point (top $S_r = 0.79$) towards the exponential equilibrium line (Fig. 8a). However, the direction of the path would depend on the actual stiffness and preconsolidation stress in the adjacent lower sections, affecting the interplay between simultaneous stress and density changes in both the top and bottom section, and on the proceeding saturation in the sample towards a potential global equilibrium in the column.

Previous studies have reported varying swelling pressure evolutions during the final stages of saturation. Lloret et al. (2003) observed a marked re-increase in swelling pressure for an initially homogeneous bentonite sample at element scale, showing a pronounced double structure behaviour, while (Villar et al., 2021) described a similar trend for layered decimetric samples composed of dense compacted bentonite and loose bentonite pellets, wherein the material response was mainly governed by the initial inhomogeneity. Dieudonné et al. (2024) amongst others showed that for an initially homogeneous material at a decimetric scale, a minimum threshold suction (or corresponding maximum degree of saturation) existed, below (or above) which no further significant swelling pressure increase was observed (Agus et al., 2013). In this context, only moderate additional stress development would be expected in the top section of the column upon full saturation.

The measured total horizontal stresses of the bottom section equally are aligned to the exponential fit of the element tests in Fig. 8a, whereas the horizontal stresses in mid and top sections are significantly below due to the incomplete saturation. The trend before the end of the test indicates a further increase in the magnitude of the radial stresses with proceeding saturation, possibly showing a more pronounced second increase in stress than the vertical stress, though no conclusion on the final magnitude can yet be drawn. Lower, or at most equal, measured final radial stresses than vertical stresses after hydration in decimetric laboratory mock-up tests were reported by Saba et al. (2014b) and Dieudonné et al. (2024) for uniaxially and isotropically compacted samples, respectively. Independent of type of compaction, hydration of the sample induced a heterogeneous stress state in the sample and a gradient in radial stresses with increasing distance from the hydration end.

Fig. 8b displays the transient wetting paths obtained from the column test together with the measured wetting paths obtained from element tests at constant volume in terms of degree of saturation versus suction. The wetting paths of the element tests correspond to Fig. 2b. In the column test, suction was derived from RH measurements at the bottom, mid and top sections during hydration (see Fig. 3) and the corresponding degree of saturation was evaluated based on the water content derived from TDR measurements at each section. Both the initial e_0 and final void ratio e_{final} were used in this calculation, since they represent limiting states for the unknown transient void ratios during hydration. In Fig. 8b they are depicted for each measuring section as solid lines for e_0 and dashed lines for e_{final} extrapolating from the known initial (solid round marker) and final state (left-filled round marker). The shadowed bandwidth indicates the potential evolution between the known initial void ratio at the start of the full line and the known final void ratio at the end of the dashed line. The paths representing the wetting SWRC in the three sections of the column test evolve close the measured SWRCs of the element tests with corresponding initial dry density. The path of the top column section clearly moved from near the medium-dense element test data ($\rho_d = 1.50 - 1.61$ g/cm^3) towards the region of higher-density element test data ($\rho_d = 1.72$ g/cm^3), corresponding well to the initial ($\rho_d = 1.54$

g/cm^3) and final measured dry density (ρ_d = 1.70 g/cm^3) of the top section, respectively (see Fig. 5). Thus, the wetting SWRC reflected the compression of the top section during hydration in the column test and the resulting shift to higher degree of saturation. A similar trend was evident for the mid column section, although the shift of the SWRC path of the mid column section is not as clear as for the top section due to the lesser compression during hydration. The inverse tendency is observed for the SWRC path of the bottom column section. It shifted from near the medium-dense element test data (ρ_d = 1.50 – 1.61 g/cm^3) down and left to the region of lower-density element test data (ρ_d = 1.41 g/cm^3), evident up to a suction of about 8 MPa. Thereafter, an assessment of the further development up to the final state is not feasible due to the lower limit of suction in the data from the element tests. However, satisfactory agreement with the final dry density of ρ_d = 1.46 g/cm^3 determined for the bottom section (Fig. 5) was evident. Thus, for all three sections, the column SWRC paths reflected the density redistribution during hydration and confirmed the consistency of the data set. In most of the previous studies, a direct evaluation of the wetting SWRC data was not possible, since water content was not measured.

6. Summary and conclusion

This work comprises an experimental study on the swelling and infiltration behaviour of uniaxially compacted Ca/Mg bentonite under constant volume conditions on different test scales. An infiltration mock-up test on decimetric scale and small-scale element tests were carried out using commercially available Calcigel to assess its material behaviour subjected to hydration for potential use as a sealing material as part of the engineered barrier system (EBS) in nuclear waste disposals. Deionized water was used as supplied fluid. Wetting from the bottom side, corresponding to the saturation conditions in the repository, was applied in all tests. The column test ran for 370 days, resulting in final degrees of saturation of 0.90, 0.81, and 0.79 in the bottom, mid and top section, respectively. The unique experimental design of the column test, including the measurement of water content alongside relative humidity, vertical and radial stresses distributed over the sample height, allowed consistent identification of hydration mechanisms in the soil sample. Therefore, a material specific calibration of the time domain reflectometry (TDR) sensors was presented. Overall, a non-uniform evolution of the hydraulic and mechanical state variables was evident over time in the column test. To validate the results and to evaluate the influence of the test scale on the swelling and water retention behaviour, the results of the column test were discussed together with those from small-scale element tests.

In the column test, the spatially resolved hydration behaviour was shown in terms of the different time evolution of relative humidity and water content. The more pronounced increase in relative humidity compared to the water content indicated a porosity redistribution within the column sample. Post-experimental sampling of the column test confirmed an evolution towards inhomogeneous distribution of dry density of the initially homogeneous compacted bentonite upon hydration. In the bottom third of the column test, the bentonite expanded, while it was compressed in the upper two thirds of the sample. Due to the partly compensating effects of the dry density increase and water content increase in the upper sections on one hand, and the dry density decrease with strong water content increase in the lower section on the other hand, the distribution of degree of saturation was, however, more uniform. A mostly anisotropic and non-uniform evolution of the swelling pressure in vertical and radial direction was evident in the column test. The magnitude of both vertical and radial stress over time was found to be dependent on the distance from the hydration end, regardless of the saturation state. The temporal development of stress is comparable to that of the water content in the sample. The measurement of vertical stress from external load cells at top and bottom rather represent the respective local stress evolution than the global behaviour of the entire sample. Measurement of the swelling pressure in the column test was influenced by effects of wall friction, evolving transient soil compressibility and additional mechanical compression stress induced by expansion of the bottom part of the column. The latter were reflected in different magnitudes of the vertical swelling pressure at lower and top end and locally within the sample. Overall, the swelling pressure near the hydration end was approximately isotropic and became more anisotropic with increasing distance from the hydration end for the final, incomplete state of saturation.

Comparison with the element test results demonstrated good agreement of externally measured vertical swelling pressure and water retention behaviour between both test scales for similar hydraulic state and dry density conditions. For a final assessment of the scale effect, further hydration in the column would be necessary. Measurement of the water content in the column test by the TDR sensors allowed for estimation of the wetting soil water retention curve and comparing it to the constant volume retention behaviour in element tests. The water retention behaviour observed in the column aligned well with the results obtained at the element scale, providing consistent evidence for the density redistribution within the column.

Local stress measurements demonstrated that swelling pressure was not uniform within the decimetric laboratory mock-up test and its development is a locally occurring process. Reliable predictions of the stress field are critical for the design of an EBS, thus the possibility of an anisotropic stress field with a radial stress gradient at increasing distance from the hydration end should be considered. In the column test, both well defined boundary conditions, together with the monitoring of transient coupled processes over time and space could be realized. Its results enabled process understanding for the design of in-situ experiments and the EBS itself. For future experiments, the test set-up of the laboratory mock-up test could benefit from a higher capacity of the embedded earth pressure transducers and the addition of local strain measurements to obtain transient data on deformation within the sample.

CRediT authorship contribution statement

Antonia Nitsch: Writing – original draft, Writing – review & editing, Visualization, Validation, Investigation, Formal analysis, Data curation, Methodology. **Ali Asaad:** Validation, Writing – review & editing. **Torsten Wichtmann:** Funding acquistion, Resources. **Katja Emmerich:** Conceptualization, Validation, Writing – review & editing, Project administration. **Wiebke Baille:** Writing – review & editing, Validation, Supervision, Conceptualization, Investigation, Project administration, Methodology.

Declaration of competing interest

The authors declare that they have no known competing financial interests or personal relationships that could have appeared to influence the work reported in this paper.

Acknowledgements

The authors are grateful to the German Federal Ministry of Economic Affairs and Energy (BMWi) for funding the project under FKZ 02E12001 A+B and to the project management Agency of Karlsruhe (PTKA) for management. Ralf Diedel at SSKG for providing the material. The laboratory staff at the Chair of Soil Mechanics, Foundation Engineering and Environmental Geotechnics at Ruhr-Universität Bochum, especially Werner Müller, for their support conducting the experiments.

Appendix A. Supplementary data

Supplementary material related to this article can be found online at https://doi.org/10.1016/j.clay.2025.108067.

References

Agus, S.S., Arifin, Y.F., Tripathy, S., Schanz, T., 2013. Swelling pressure-suction relationship of heavily compacted bentonite-sand mixtures. Acta Geotech. 8 (2), 155–165. http://dx.doi.org/10.1007/s11440-012-0189-0.

Agus, S.S., Schanz, T., 2008. A method for predicting swelling pressure of compacted bentonites. Acta Geotech. 3 (2), 125–137. http://dx.doi.org/10.1007/s11440-008-0057-0.

Akesson, M., Jacinto, A.C., Gatabin, C., Sanchez, M., Ledesma, A., 2009. Bentonite THM behaviour at high temperatures: Experimental and numerical analysis. Geotechnique 59 (4), 307–318. http://dx.doi.org/10.1680/geot.2009.59.4.307, URL: https://www.scopus.com/inward/record.uri?eid=2-s2.0-65249172082&doi=10.1680%2fgeot.2009.59.4.307&partnerID=40&md5=f0ed2689d7683333327872be3db51d33.

Asaad, A., Nitsch, A., Baille, W., Emmerich, K., 2025. Mineralogical and geotechnical characterization of two German bentonites from Westerwald and Bavaria. Appl. Clay Sci. 276, 107901. http://dx.doi.org/10.1016/j.clay.2025.107901, https://www.sciencedirect.com/science/article/pii/S0169131725002066.

Baille, W., Tripathy, S., Schanz, T., 2010. Swelling pressures and one-dimensional compressibility behaviour of bentonite at large pressures. Appl. Clay Sci. 48 (3), 324–333, URL: http://www.sciencedirect.com/science/article/pii/S0169131710000037.

Bernachy-Barbe, F., 2021. Homogenization of bentonite upon saturation: Density and pressure fields. Appl. Clay Sci. 209, 106122. http://dx.doi.org/10.1016/j.clay.2021.106122, URL: https://www.sciencedirect.com/science/article/pii/S0169131721001460.

Bernachy-Barbe, F., Conil, N., Guillot, W., Talandier, J., 2020. Observed heterogeneities after hydration of MX-80 bentonite under pellet/powder form. Appl. Clay Sci. 189, 105542. http://dx.doi.org/10.1016/j.clay.2020.105542, URL: https://www.sciencedirect.com/science/article/pii/S0169131720301071.

Brunauer, S., Emmett, P.H., Teller, E., 1938. Adsorption of gases in multimolecular layers. J. Am. Chem. Soc. 60 (2), 309–319. http://dx.doi.org/10.1021/ja01269a023.

Bucher, F., Müller-Vonmoos, M., 1989. Bentonite as a containment barrier for the disposal of highly radioactive wastes. Appl. Clay Sci. 4 (2), 157–177. http://dx.doi.org/10.1016/0169-1317(89)90006-9, URL: https://www.sciencedirect.com/science/article/pii/0169131789900069.

Bucher, F., Spiegel, U., 1984. Quelldruck von hochverdichteten Bentoniten. Technical Report 84–18, Nagra, Institut für Grundbau und Bodenmechanik, ETH Zürich.

Carter, D., Heilman, M., Gonzales, C., 1965. Ethylene glycol monoethyl ether for Determining Surface Area of silicate minerals. Soil Sci. 100 (5), 356–360.

Cerato, A., Lutenegger, A., 2002. Determination of surface area of fine-grained soils by the ethylene glycol monoethyl ether (EGME) method. Geotech. Test. J. - GEotech. Testing J. 25, http://dx.doi.org/10.1520/GTJ11087J.

Chang, C., Borglin, S., Chou, C., Zheng, L., Wu, Y., Kneafsey, T.J., Nakagawa, S., Voltolini, M., Birkholzer, J.T., 2023. Hydro-mechanical behavior of heated bentonite buffer for geologic disposal of high-level radioactive waste: A bench-scale X-ray computed tomography investigation. Appl. Clay Sci. 232, 106792. http://dx.doi.org/10.1016/j.clay.2022.106792, URL: https://www.sciencedirect.com/science/article/pii/S0169131722003878.

Christ, F., Lieske, W., Herz, C., Wichtmann, T., 2022. Evaluation of the penetration behavior of viscous fluids into porous media in the context of volume determination. Geotech. Test. J. 45, 18. http://dx.doi.org/10.1520/GTJ20210213.

Cui, Y.J., 2017. On the hydro-mechanical behaviour of MX80 bentonite-based materials. J. Rock Mech. Geotech. Eng. 9 (3), 565–574. http://dx.doi.org/10.1016/j.jrmge.2016.09.003, URL: https://www.sciencedirect.com/science/article/pii/S1674775516300555.

Daniels, K.A., Harrington, J.F., Sellin, P., Norris, S., 2021. Closing repository void spaces using bentonite: does heat make a difference? Appl. Clay Sci. 210, 106124. http://dx.doi.org/10.1016/j.clay.2021.106124, URL: https://www.sciencedirect.com/science/article/pii/S0169131721001484.

Darde, B., Tang, A.M., Pereira, J.M., Dangla, P., Roux, J.N., Chabot, B., Talandier, J., Vu, M.N., 2022. Influence of heterogeneities of density on the hydromechanical behaviour of pellet-based bentonite materials in imbibition experiments. Appl. Clay Sci. 216, 106353. http://dx.doi.org/10.1016/j.clay.2021.106353, URL: https://www.sciencedirect.com/science/article/pii/S016913172100377X.

Delage, P., Cui, Y., Tang, A.M., 2010. Clays in radioactive waste disposal. J. Rock Mech. Geotech. Eng. 2, 111–123. http://dx.doi.org/10.3724/SP.J.1235.2010.00111.

Dieudonné, A.C., Gatabin, C., Dridi, W., Talandier, J., Collin, F., Charlier, R., 2024. Heterogeneous swelling of an isotropically compacted bentonite-based material: Experimental observations and modelling. Rock Mech. Rock Eng. 57 (6), 4159–4172. http://dx.doi.org/10.1007/s00603-023-03476-z.

DIN 18196:2023-02, 2023. Earthworks and Foundations - Soil Classification for Civil Engineering Purposes. Deutsches Institut für Normung, DIN, Beuth, Berlin, http://dx.doi.org/10.31030/3395928.

DIN EN ISO 17892-4:2017-04, 2017. Geotechnical Investigation and Testing - Laboratory Testing of Soil - Part 4: Determination of Particle Size Distribution (ISO 17892-4:2016); German Version EN ISO 17892-4:2016. Deutsches Institut für Normung, DIN, Beuth, Berlin, http://dx.doi.org/10.31030/2362539.

Emmerich, K., Kemper, G., Königer, F., Schlaeger, S., Gruner, M., Gaßner, W., Hofmann, M., Nüesch, R., Schuhmann, R., 2009. Saturation kinetics of a vertical multilayer hydraulic sealing system exposed to rock salt brine. Vadose Zone J. - Vadose Zone J. 8, http://dx.doi.org/10.2136/vzj2008.0094.

Emmerich, K., Königer, F., Kaden, H., Thissen, P., 2015. Microscopic structure and properties of discrete water layer in na-exchanged montmorillonite. J. Colloid Interface Sci. 448C, http://dx.doi.org/10.1016/j.jcis.2015.01.087.

Emmerich, K., Schuhmann, R., Koeniger, F., Bohac, P., Delavernhe, L., Wieczorek, K., Czaikowski, O., Hesser, J., Shao, H., Jaeggi, D., 2019. Joint Project: Vertical Hydraulic Sealing System Based on the Sandwich Principle–Preproject (Sandwich-VP). Technical Report, Karlsruher Institut für Technologie (KIT) & Gesellschaft für Anlagen- und Reaktorsicherheit (GRS) gGmbH.

Enresa, 2006. FEBEX-Full-scale Engineered Barriers Experiment, Updated Final Report 1994–2004. Publicación técnica 05-0/2006, Empresa Nacional de Residuos Radiactivos, Madrid.

García-Siñeriz, J.L., Rey Mazón, M., Mayor, J.C., 2008. The engineered barrier experiment at mont terri rock laboratory. Andra, Sci. Technol. Ser. 334, 65–75.

García-Siñeriz, J.L., Villar, M.V., Rey, M., Palacios, B., 2015. Engineered barrier of bentonite pellets and compacted blocks: State after reaching saturation. Eng. Geol. 192, 33–45. http://dx.doi.org/10.1016/j.enggeo.2015.04.002, URL: https://www.sciencedirect.com/science/article/pii/S001379521500109X.

Harrington, J., Daniels, K., Wiseall, A., Sellin, P., 2020. Bentonite homogenisation during the closure of void spaces. Int. J. Rock Mech. Min. Sci. 136, http://dx.doi.org/10.1016/j.ijrmms.2020.104535.

Jacinto, A., Villar, M., Ledesma, A., 2012. Influence of water density on the water-retention curve of expansive clays. Géotechnique 62, 657–667. http://dx.doi.org/10.1680/geot.7.00127.

Koeniger, F., Emmerich, K., Kemper, G., Gruner, M., Gassner, W., Nueesch, R., Schuhmann, R., 2008. Moisture spreading in a multi-layer hydraulic sealing system (HTV-1). Eng. Geol. 98 (1), 41–49. http://dx.doi.org/10.1016/j.enggeo.2008.01.001, URL: https://www.sciencedirect.com/science/article/pii/S001379520800015X.

Lang, L.Z., Tripathy, S., Baille, W., Schanz, T., Sridharan, A., 2019. Linkage between swelling pressure, total suction of saturated bentonites and suction of saturating aqueous solutions. Appl. Clay Sci. 171, 82–91. http://dx.doi.org/10.1016/j.clay.2019.02.007, URL: http://www.sciencedirect.com/science/article/pii/S0169131719300377.

Lee, J.O., Lim, J.G., Kang, I.M., Kwon, S., 2012. Swelling pressures of compacted Ca-bentonite. Eng. Geol. 129–130, 20–26. http://dx.doi.org/10.1016/j.enggeo.2012.01.005, URL: https://www.sciencedirect.com/science/article/pii/S0013795212000178.

Leong, E.C., Tripathy, S., Rahardjo, H., 2003. Total suction measurement of unsaturated soils with a device using the chilled-mirror dew-point technique. Géotechnique 53 (2), 173–182. http://dx.doi.org/10.1680/geot.2003.53.2.173, arXiv:https://doi.org/10.1680/geot.2003.53.2.173.

Lloret, A., Villar, M.V., Sánchez, M., Gens, A., Pintado, X., Alonso, E.E., 2003. Mechanical behaviour of heavily compacted bentonite under high suction changes. Géotechnique 53 (1), 27–40. http://dx.doi.org/10.1680/geot.2003.53.1.27, URL: https://www.icevirtuallibrary.com/doi/abs/10.1680/geot.2003.53.1.27.

Martín, P.L., Barcala, J.M., 2005. Large scale buffer material test: Mock-up experiment at CIEMAT. Eng. Geol. 81 (3), 298–316. http://dx.doi.org/10.1016/j.enggeo.2005.06.013, URL: https://www.sciencedirect.com/science/article/pii/S0013795205001328.

Mokni, N., Barnichon, J.D., 2016. Hydro-mechanical analysis of SEALEX in-situ tests – impact of technological gaps on long term performance of repository seals. Eng. Geol. 205, 81–92. http://dx.doi.org/10.1016/j.enggeo.2016.02.013, URL: https://www.sciencedirect.com/science/article/pii/S0013795216300461.

Monroy, R., Zdravkovic, L., Ridley, A., 2010. Evolution of microstructure in compacted London clay during wetting and loading. Géotechnique 60 (2), 105–119. http://dx.doi.org/10.1680/geot.8.P.125, arXiv:https://doi.org/10.1680/geot.8.P.125.

Nagra, 2002. Projekt Opalinuston: Konzept für die Anlage und den Betrieb eines geologischen Tiefenlagers– Entsorgungsnachweis für abgebrannte Brennelemente, verglaste hochaktive sowie langlebige mittelaktive Abfälle. Technical Report, Nagra, Wettingen, Switzerland.

Navarro, V., Cabrera, V., Merlo, O., De la Morena, G., Torres-Serra, J., 2022. Density of water adsorbed on bentonites: Determination and effect on microstructural void ratio modelling. Appl. Clay Sci. 219, 106434. http://dx.doi.org/10.1016/j.clay.2022.106434, URL: https://www.sciencedirect.com/science/article/pii/S0169131722000291.

Nitsch, A., Leuthold, J., Machaček, J., Grandas Tavera, C.E., 2023. Experimental investigations on hydro-mechanical processes in reconstituted clay shale and their significance for constitutive modelling. Rock Mech. Rock Eng. 56 (4), 2457–2478. http://dx.doi.org/10.1007/s00603-022-03202-1.

Nüesch, R., Brandelik, A., Hübner, C., Schuhmann, R., 2002. Verschlussstopfen und Verfahren zum Verschließen von untertägigen Hohlräumen. Technical Report, KIT, Karlsruhe.

Pusch, R., 1977. KBS:Technical Report 33: Required Physical and Mechanical Properties of Buffer Masses. Technical Report, Swedish Nuclear Fuel Supply Co, Stockholm.

Rawat, A., 2019. Coupled Hydro-mechanical Behavior of a Compacted Bentonite-Sand Mixture: Experimental and Numerical Investigations (Ph.D. thesis). Ruhr-Universität Bochum, Universitätsbibliothek.

Rawat, A., Baille, W., Tripathy, S., 2019. Swelling behavior of compacted bentonite-sand mixture during water infiltration. Eng. Geol. 257, 105141. http://dx.doi.org/10.1016/j.enggeo.2019.05.018, URL: https://www.sciencedirect.com/science/article/pii/S001379521831055X.

Rawat, A., Baille, W., Tripathy, S., Schanz, T., 2021. A column-type experimental device for investigating coupled thermo-hydro-mechanical behavior of expansive soils. Geotech. Test. J. 44, http://dx.doi.org/10.1520/GTJ20180192.

Romero, E., 1999. Characterisation and Thermo-Hydro-Mechanical Beha-Viour of Unsaturated Boom Clay: An Experimental Study (Ph.D. thesis). Univ. Polytec. de Catalunya , Barcelona, Spain..

Romero, E., Della Vecchia, G., Jommi, C., 2011. An insight into the water retention properties of compacted clayey soils. Géotechnique 61 (4), 313–328. http://dx.doi.org/10.1680/geot.2011.61.4.313, arXiv:https://doi.org/10.1680/geot.2011.61.4.313.

Saba, S., Barnichon, J.D., Cui, Y.J., Tang, A.M., Delage, P., 2014a. Microstructure and anisotropic swelling behaviour of compacted bentonite/sand mixture. J. Rock Mech. Geotech. Eng. 6, http://dx.doi.org/10.1016/j.jrmge.2014.01.006.

Saba, S., Cui, Y.J., Tang, A.M., Barnichon, J.D., 2014b. Investigation of the swelling behaviour of compacted bentonite-sand mixture by mock-up tests. Can. Geotech. J. 51, 1399–1412. http://dx.doi.org/10.1139/cgj-2013-0377.

Sandén, T., Goudarzi, R., de Combarieu, M., Åkesson, M., Hökmark, H., 2007. Temperature buffer test – design, instrumentation and measurements. Phys. Chem. Earth 32, 77–92, URL: https://api.semanticscholar.org/CorpusID:128558559.

Schanz, T., Baille, W., Long, N.T., 2011. Effects of temperature on measurements of soil water content with time domain reflectometry. Geotech. Test. J. 34 (1), 1–8. http://dx.doi.org/10.1520/GTJ103152.

Schanz, T., Tripathy, S., 2009. Swelling pressure of a divalent-rich bentonite: Diffuse double-layer theory revisited. Water Resour. Res. 45 (5), http://dx.doi.org/10.1029/2007WR006495.

Schuhmann, R., Emmerich, K., Kemper, G., Koeniger, F., 2009. Verschlusssystem mit Äquipotenzialsegmenten für die Untertägige Entsorgung (UTD und ELA) Gefährlicher Abfälle zur Sicherherstellung der Homogenen Befeuchtung der Dichtelemente und zur Verbesserung der Langzeitstabilität: Schlussbericht. Technical Report, Karlsruher Institut für Technologie: Karlsruhe, Germany.

Seiphoori, A., Ferrari, A., Laloui, L., 2014. Water retention behaviour and microstructural evolution of MX-80 bentonite during wetting and drying cycles. Géotechnique 64 (9), 721–734. http://dx.doi.org/10.1680/geot.14.P.017, URL: https://www.icevirtuallibrary.com/doi/abs/10.1680/geot.14.P.017.

Skierucha, W., 2009. Temperature dependence of time domain reflectometry-measured soil dielectric permittivity. J. Plant Nutr. Soil Sci. 172, 574–582.

Vaunat, J., Gens, A., 2005. Analysis of the hydration of a bentonite seal in a deep radioactive waste repository. Eng. Geol. 81 (3), 317–328. http://dx.doi.org/10.1016/j.enggeo.2005.06.014, URL: https://www.sciencedirect.com/science/article/pii/S001379520500133X.

Villar, M.V., Iglesias, R.J., Gutiérrez-Álvarez, C., Carbonell, B., 2021. Pellets/block bentonite barriers: Laboratory study of their evolution upon hydration. Eng. Geol. 292, 106272. http://dx.doi.org/10.1016/j.enggeo.2021.106272, URL: https://www.sciencedirect.com/science/article/pii/S0013795221002830.

Wang, H., 2024. Pore water density in a saturated bentonite. Geotechnique 74 (12), 1254–1262. http://dx.doi.org/10.1680/jgeot.22.00247.

Wang, Q., Cui, Y.J., Tang, A.M., Barnichon, J.D., Saba, S., Ye, W.M., 2013. Hydraulic conductivity and microstructure changes of compacted bentonite/sand mixture during hydration. Eng. Geol. 164, 67–76. http://dx.doi.org/10.1016/j.enggeo.2013.06.013.

Wieczorek, K., Emmerich, K., Nagel, T., Bakker, E., Diedel, R., Furche, M., García-Siñeriz, J.L., Glaubach, U., Hesser, J., Hinze, M., Jaeggi, D., Koeniger, F., Mayor Zurdo, J.C., Raebiger, L., Rey Mazon, M., Roelke, C., Schaedle, P., Schuhmann, R., Shao, H., Tunon, S., Victoria Villar Galicia, M., Wilsnack, T., Yeatman, R., 2024. Sandwich-HP - Vertical Hydraulic Sandwich Sealing System–Final report. Technical Report GRS-745, Gesellschaft für Anlagen- und Reaktorsicherheit (GRS) gGmbH.

Wieczorek, K., Emmerich, K., Schuhmann, R., Hesser, J., Furche, M., Jaeggi, D., Schefer, S., Aurich, J., Mayor, J.C., Norris, S., Birch, K., Sentis, M., García-Siñeriz, J.L., Koeniger, F., Glaubach, U., Roelke, C., Diedel, R., 2021. Large-scale testing of a sandwich shaft-sealing system at the mont terri rock laboratory. 1, pp. 133–135. http://dx.doi.org/10.5194/sand-1-133-2021, URL: https://sand.copernicus.org/articles/1/133/2021/,

Wu, T., Cleall, P., Tripathy, S., 2024. A constitutive model considering the interaction between evolution of microstructure and hydro-mechanical behaviour of unsaturated soils. Comput. Geotech. 176, 106775. http://dx.doi.org/10.1016/j.compgeo.2024.106775.